Applied Science and Engineering Progress, Vol. 20, No. 2, 2027, 8141

Research Article

Investigation of oxygen permeation behavior across BYS-coated LSCF Multi-Channel Hollow Fiber Membrane using N_2O as an Oxygen Source

Issara Sereewatthanawut
King Prajadhipok's Institute, Bangkok 10210, Thailand.
Bangkok Thonburi University, 16/10 Leabklongtaweewatana Road, Taweewatana, Bangkok 10170, Thailand.

Vut Tongnan, Notsawan Swadchaipong, Chalempol Khajonvittayakul, Ammarika Makdee, Rawisara Tuncharoen, Panupun Maneesard and Unalome Wetwatana Hartley*
Chemical and Process Engineering, The Sirindhorn International Thai-German Graduate School of Engineering (TGGS), King Mongkut's University of Technology North Bangkok, Bangkok, 10800, Thailand.

Kang Li
Chemical Engineering, Imperial College London, UK, SW7 2AZ.

Matthew Hartley
Department of Chemical Engineering, Faculty of Engineering, King Mongkut's University of Technology North Bangkok, Bangkok, 10800, Thailand.

* Corresponding author. E-mail: unalome.w.cpe@tggs-bangkok.org DOI: 10.14416/j.asep.2026.07.010
Received: 12 November 2025; Revised: 12 February 2026; Accepted: 18 February 2026; Published online: 23 July 2026

Abstract

A 6-channel LSCF hollow fiber membrane was successfully fabricated and subsequently modified via an *in situ* coating of BYS to enhance its oxygen transport performance. The BYS coating formed a uniform, thin film along the inner surface of the LSCF membrane, increasing surface roughness and active site density for oxygen exchange without compromising mechanical integrity. Oxygen permeation experiments were carried out using both air and N_2O as oxygen sources. Under air feed conditions, the BYS-modified membrane exhibited a markedly higher oxygen permeation flux than the pristine LSaCF membrane, confirming that the BYS layer effectively promoted surface exchange kinetics. When N_2O was employed, the oxygen permeation rate was strongly dependent on both gas flow rate and operating temperature. Under optimized conditions (50 mL/min of N_2O feed and 100 mL/min of Ar sweep gas), the BYS-coated LSCF membrane achieved an oxygen permeation flux of 2.0 mL/min·cm^2 with 80% N_2O conversion at 980 °C. These findings demonstrate the beneficial relationship between N_2O decomposition and *in situ* oxygen removal, establishing the BYS-coated LSCF hollow fiber as a highly efficient oxygen transport platform and a promising, sustainable pathway for greenhouse gas mitigation.

Keywords: BYS coating, Hollow fiber membrane, LSCF membrane, N_2O decomposition, Oxygen permeation

1 Introduction

Mixed ionic-electronic conducting (MIEC) oxide-based oxygen-permeable ceramic membranes have attracted considerable attention for high-temperature applications, requiring a controlled oxygen supply, such as the oxidative coupling of methane [1-3], selective oxidation of hydrocarbons [4], and syngas production [5]. These membranes facilitate selective oxygen ion transport driven by a chemical potential gradient, thereby enabling oxygen separation without the use of external electrodes. Consequently, they provide a simpler and more energy-efficient alternative to conventional oxygen separation

Applied Science and Engineering Progress, Vol. 20, No. 2, 2027, 8141

technologies, such as cryogenic distillation and pressure swing adsorption [6]. In addition to their high oxygen selectivity, MIEC membranes facilitate process intensification by integrating oxygen separation and catalytic reaction within a single reactor unit, reducing operational complexity and improving overall efficiency [7].

Among various MIEC materials, perovskite-type oxides with the general formula $ABO_{3-\delta}$ (where A and B are metal cations and δ denotes oxygen vacancies) have been extensively studied for oxygen separation. Their transport performance can be tuned through partial substitution at the A and/or B sites, yielding compositions such as $A_{1-x}A'_xB_{1-y}B'_yO_{3-\delta}$. Such substitution enhances oxygen vacancy concentration and promotes oxide-ion mobility within the lattice [8]. In particular, $La_{0.6}Sr_{0.4}Co_{0.2}Fe_{0.8}O_{3-\delta}$ (LSCF) has been widely studied due to its high oxygen permeability, favorable redox behavior, mechanical robustness, and compatibility with various membrane configurations [9], [10]. LSCF membranes can be fabricated in planar, tubular, or hollow fiber geometries, with hollow fibers offering distinct advantages, including thinner separation layers, higher surface area-to-volume ratios, and improved mechanical integrity. These features contribute to enhanced oxygen flux compared with planar and tubular counterparts [11], [12]. Nevertheless, the oxygen permeation performance of LSCF membranes is often limited by sluggish surface exchange kinetics, particularly under low oxygen partial pressures or when alternative oxygen sources are employed [13]. To overcome this limitation, various surface modification strategies have been proposed, such as the deposition of porous catalytic overlayers to increase active surface area and the application of oxygen-conducting materials to accelerate surface exchange reactions [13-15].

$Bi_{1.5}Y_{0.3}Sm_{0.2}O_{3-\delta}$ (BYS), a co-doped derivative of the cubic fluorite δ-Bi_2O_3 phase, is recognized for its exceptionally high oxide-ion conductivity. Although pure δ-Bi_2O_3 exhibits one of the highest ionic conductivities among bismuth-based oxides, its structural stability is restricted to a narrow temperature range (730-825 °C), beyond which it transforms into less conductive polymorphs [16], [17]. Doping with rare-earth cations such as Y^{3+} and Sm^{3+} stabilizes the δ-phase and enhances oxygen-ion mobility at elevated temperatures [18]. In addition, BYS exhibits favorable interfacial compatibility with LSCF and promotes faster oxygen surface exchange kinetics, which helps reduce surface exchange resistance. Othman et al. [19] reported that BYS maintains its fluorite structure up to 1040 °C under oxidative coupling of methane (OCM) conditions. Furthermore, the use of BYS as a surface modification layer on LSCF membranes has been shown to enhance both oxygen permeation and OCM performance through improved ionic transport and strong interfacial interactions between BYS and LSCF phases [20]. These results suggest that BYS is a promising oxygen-conductive coating material capable of simultaneously improving catalytic activity and oxygen permeability in an integrated membrane system.

In addition to conventional oxygen sources such as air, nitrous oxide (N_2O) has recently emerged as a potential alternative feed for oxygen-permeable membranes. Anthropogenic N_2O emissions primarily originate from agricultural activities, fossil-fuel combustion, and industrial processes such as nitric acid and adipic acid production [21], [22]. N_2O is a potent greenhouse gas, contributing to ozone layer depletion [23] and exhibiting a global warming potential approximately 273 times greater than that of CO_2 over a 100-year time horizon [24]. Therefore, effective N_2O mitigation strategies are of significant environmental importance. Various approaches, including thermal decomposition, selective adsorption, and catalytic decomposition, have been explored [25]. Among these, catalytic decomposition is particularly attractive due to its moderate energy requirements and the generation of oxygen as a valuable byproduct. However, conventional catalysts, such as noble metal oxides, transition metal oxides, and perovskite-type compounds, often suffer from surface oxygen accumulation, which inhibits reaction kinetics. Integrating perovskite-type MIEC membranes into this process provides a promising solution, as the membrane can catalyze N_2O decomposition while simultaneously removing the generated oxygen through dense ionic transport. This continuous oxygen extraction mitigates surface inhibition and produces a high-purity oxygen stream [26]. Such dual functionality enhances both N_2O conversion and oxygen recovery, offering a sustainable pathway for greenhouse gas abatement. Nevertheless, further optimization of membrane composition and architecture is required to achieve high oxygen flux, strong catalytic performance, and long-term operational stability under harsh conditions. In this study, a 6-channel LSCF hollow fiber membrane was fabricated via a phase inversion-sintering method and subsequently modified through in-situ deposition of a BYS layer

to enhance surface oxygen exchange and catalytic performance. The structure, morphology, and oxygen transport behavior of the synthesized membrane were systematically examined. Oxygen permeation experiments were conducted using both synthetic air and N_2O as oxygen sources. For N_2O operation, particular attention was given to the interplay between catalytic N_2O decomposition and in situ oxygen removal under varying feed flow rates, sweep gas flow rates, and operating temperatures. The results demonstrate the potential of BYS-modified LSCF hollow fiber membranes as multifunctional systems for efficient oxygen delivery and simultaneous greenhouse gas mitigation.

2 Materials and Methods

2.1 *Fabrication of 6-channel LSCF hollow fiber membrane*

The 6-channel LSCF hollow fiber membrane was fabricated using a phase inversion-sintering technique [27]. The spinning suspension comprised 63.7 wt% LSCF powder, 7.1 wt% polyethersulfone (PESf), 28.5 wt% dimethyl sulfoxide (DMSO), and 0.6 wt% Arlacel P135 as dispersant. All components except PESf were initially ball-milled in a planetary mill for 24 h. Subsequently, PESf was added, and milling continued for an additional 72 h to ensure complete homogenization. The resulting suspension was degassed under vacuum to eliminate trapped air bubbles and then transferred into a 200 mL stainless steel syringe. Fiber spinning was carried out using a syringe pump equipped with a customized 6-channel spinneret featuring a tube-in-orifice and triple-orifice configuration. The ceramic suspension was extruded at a flow rate of 9 mL/min through a 1 cm air gap into a deionized water coagulation bath. Simultaneously, deionized water was introduced as the bore fluid at 15 mL/min to form the internal channels. The as-spun green fibers were immersed in deionized water overnight to complete phase inversion. The fibers were then cut to the desired length, straightened, and air-dried for 48 h. Thermal treatment was performed in two stages. First, the dried fibers were calcined at 600 °C for 2 h to remove the polymer binder. Subsequently, sintering was conducted at 1300 °C for 5 h to achieve densification and form the final 6-channel hollow fiber membrane structure. The heating rate during calcination and sintering was maintained at 10 °C/min in an air atmosphere.

2.2 *In situ BYS coating on 6-channel LSCF hollow membrane*

BYS was synthesized using a citrate sol-gel method. Metal nitrate precursors, including $Bi(NO_3)_3{\cdot}5H_2O$, $Y(NO_3)_3{\cdot}4H_2O$, and $Sm(NO_3)_3{\cdot}6H_2O$ were dissolved in dilute nitric acid. Citric acid and ethylene glycol were then added at a molar ratio of 1:2:3 (total metal ions: citric acid: ethylene glycol). The solution was stirred at 75 °C for 5 h to promote polyesterification and the formation of a homogeneous polymeric network. The prepared sol was injected into the internal channels of the 6-channel LSCF hollow fiber using a high-pressure syringe pump at a flow rate of 0.5 mL/min. Excess sol was removed from the lumen, and the coated fibers were dried overnight under ambient conditions. The samples were subsequently calcined at 400 °C for 2 h to eliminate organic components and further heated to 800 °C for 5 h to crystallize the BYS coating layer.

2.3 *Oxygen permeation test*

Figure 1 illustrates the schematic diagram of the laboratory-scale membrane reactor. A 30 cm long hollow fiber membrane was mounted inside a quartz tube and placed in an electrically heated furnace. Oxygen permeation experiments were conducted at atmospheric pressure over a temperature range of 800-980 °C. The oxygen source (synthetic air or N_2O) was supplied to the shell side of the membrane, while argon (Ar) was introduced to the lumen side as a sweep gas to establish an oxygen partial pressure gradient across the membrane. All gas flow rates were precisely controlled using mass flow controllers. The effects of operating temperature, N_2O feed flow rate, and Ar sweep gas flow rate on membrane performance

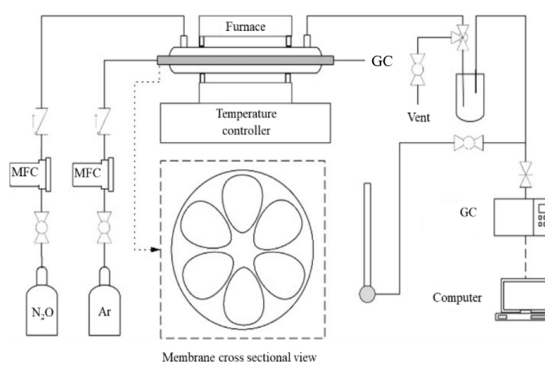

Figure 1: Experimental setup schematic for evaluating oxygen permeation.

were systematically investigated. The outlet gas compositions from both the shell and lumen sides were analyzed online using a gas chromatograph (Varian 3900). Volumetric flow rates were determined using calibrated bubble flow meters. The oxygen permeation flux (J_{O_2}) was calculated according to Equation (1):

$$J_{O_2}=\frac{V_{Ar}y_{O_2}}{A_0(100-y_{O_2})} \quad (1)$$

where V_{Ar} is the volumetric flow rate of the argon sweep gas (mL/min), y_{O_2} is the oxygen concentration (%) determined by GC analysis, and A_0 represents the external surface area of the membrane (cm²).

2.4 *Characterizations*

The crystalline phases of the synthesized materials were analyzed using X-ray diffraction (XRD) with a Rigaku SmartLab SE diffractometer equipped with a D/teX Ultra 250 detector and Cu K_α radiation (λ = 1.5410 Å), operated at 40 kV and 100 mA. Diffraction patterns were collected over a 2θ range of 20-80°, with a step size of 0.01° and a scan rate of 5°/min. Prior to analysis, membrane samples were ground into fine powders. Membrane morphology and BYS layer deposition were examined using a JEOL JSM-5610LV scanning electron microscope (SEM) operating in secondary electron (SE) mode. The BYS deposition within the membrane channels was further investigated using a high-resolution field-emission scanning electron microscope (FESEM, Gemini 1525). Before SEM observation, all samples were coated with a thin layer of gold under vacuum to enhance electrical conductivity.

3 Results and Discussion

3.1 *Material characterizations*

3.1.1 X-ray diffraction (XRD)

The XRD patterns of BYS powder, LSCF powder, and the BYS-coated LSCF hollow fiber membrane (in powdered form) are displayed in Figure 2. The BYS sample exhibited main diffraction peaks at 2θ = 28.0°, 32.5°, 46.7°, and 55.3°, corresponding to the (111), (200), (220), and (311) planes of the cubic fluorite δ-Bi_2O_3 phase (JCPDS No. 27-0052) [28], [29]. These

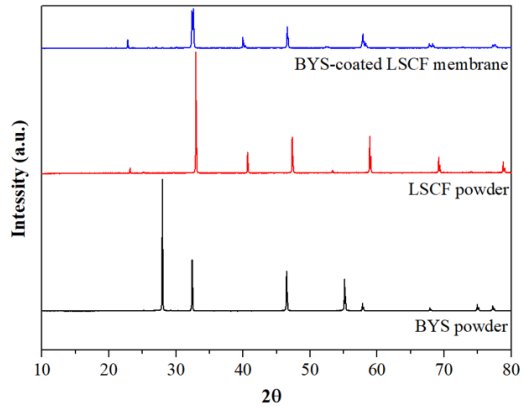

Figure 2: BYS powder, LSCF powder, and BYS-coated LSCF membrane XRD patterns.

results confirm that Y^{3+} and Sm^{3+} were successfully incorporated into the Bi_2O_3 lattice, stabilizing the highly conductive δ-phase structure. The LSCF powder exhibited characteristic diffraction peaks at 2θ = 33.0°, 40.8°, 47.3°, 58.8°, 69.3°, and 78.9°, indexed to the (110), (202), (024), (214), (208), and (128) planes of the perovskite structure (JCPDS No. 49-285) [30], [31]. The absence of secondary phases in both materials confirms successful synthesis of single-phase BYS and LSCF. For the BYS-coated LSCF membrane, the diffraction pattern was dominated by the LSCF perovskite peaks, indicating that spinning, sintering, and in situ coating did not alter the bulk crystal structure of the substrate [11]. No distinct BYS reflections were detected, which is attributed to the thin coating layer being below the XRD detection limit. Moreover, the absence of additional peaks suggests that no undesirable secondary phases or interfacial reactions occurred during fabrication. Compared with pristine powders, the coated membrane exhibited slightly reduced peak intensities and minor shifts toward lower 2θ values. This behavior may be associated with lattice strain induced during the coating process, potentially causing slight lattice expansion and variation in the lattice parameter [32].

3.1.2 Morphology of the hollow fiber membrane

SEM images of the 6-channel LSCF hollow fiber membrane are shown in Figure 3. The membrane consists of six parallel internal channels with an average outer diameter of 1.95 ± 0.03 mm (Figure 3a).

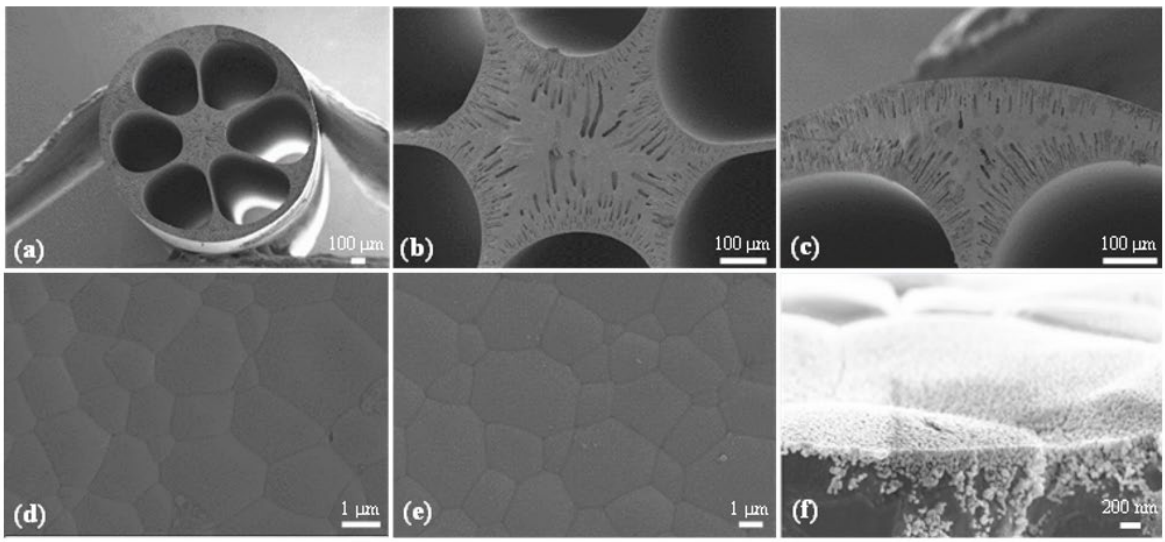

Figure 3: SEM images of the 6-channel LSCF hollow membrane : (a) whole view, (b) cross-sectional SEM images, (c) border of active region for oxygen permeation, (d) inside surface, (e) outside surface, and (f) BYS layer coating inside the channels.

This multi-channel configuration enhances mechanical robustness and thermal stability during high-temperature operation while providing a higher surface-area-to-volume ratio compared with single-channel designs [33]. Cross-sectional images (Figures 3b and 3c) reveal a porous wall structure, which facilitates gas diffusion and supports efficient oxygen-ion transport. The porous architecture also promotes effective infiltration and adhesion of secondary catalytic layers, improving gas–solid interaction [34]. The inner and outer surfaces (Figures 3d and 3e) appear smooth and defect-free, without observable cracks or pinholes, confirming adequate densification during sintering. After coating, a continuous BYS layer approximately 200 nm thick was observed along the inner channel walls (Figure 3f). The coating exhibited good adhesion to the LSCF substrate, with no signs of delamination or microcracking. The increased surface roughness and expanded interfacial area introduced by the BYS layer are expected to enhance oxygen surface exchange kinetics [35]. The synergistic combination of the oxygen-conductive BYS layer and the mechanically stable LSCF substrate therefore provides a structurally robust and catalytically active membrane platform.

3.2 *Oxygen permeation behavior of the 6-channel hollow fiber membrane*

The oxygen transport properties of the fabricated 6-channel hollow fiber membranes were systematically investigated using two oxygen sources: air and nitrous oxide (N_2O). Air provides a stable and continuous oxygen supply and was therefore used as a reference to evaluate the intrinsic oxygen transport characteristics of the membrane. In contrast, N_2O acts as an oxygen donor via catalytic decomposition, while simultaneously offering the environmental benefit of mitigating potent greenhouse gases. Comparison of these two oxygen sources provides deeper insight into the underlying transport mechanisms and highlights the membrane's potential for sustainable catalytic applications.

3.2.1 Oxygen permeation using air: effect of temperature and BYS modification

The oxygen permeation performance of the 6-channel LSCF hollow fiber membrane with and without a BYS coating was evaluated under identical operating conditions. As shown in Figure 4(a), measurements were conducted over a temperature range of 800-950 °C, with 100 mL/min of air supplied to the shell side and an equal flow rate of argon (Ar) introduced to the lumen side as the sweep gas.

For both membrane configurations, the oxygen permeation flux increased steadily with temperature, confirming that oxygen surface exchange and bulk

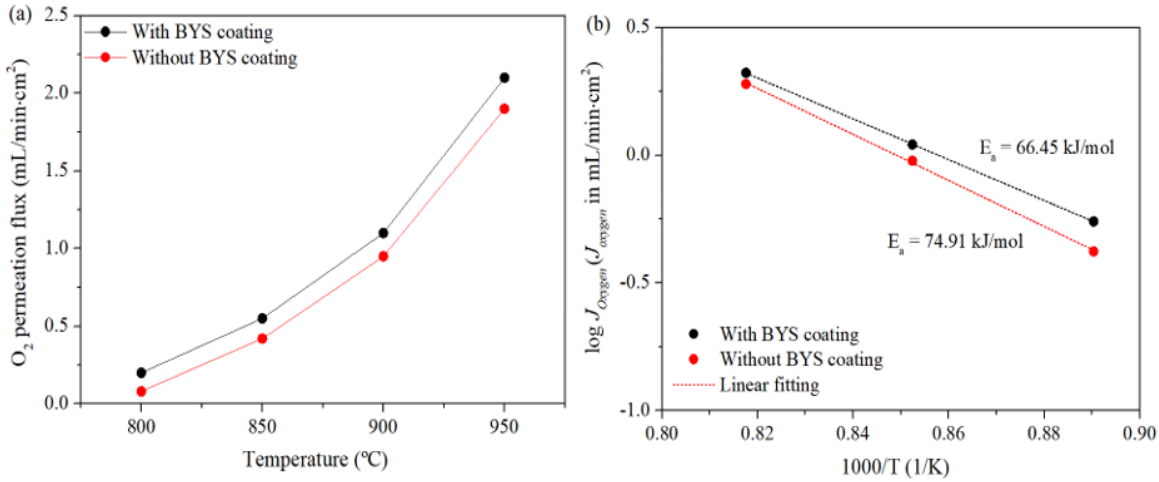

Figure 4: **(a)** Oxygen permeation fluxes across the uncoated and BYS-coated LSCF hollow membranes at various temperatures (800-950 °C). **(b)** Arrhenius plots for the uncoated and BYS-coated LSCF membranes at different temperatures (800-950 °C).

oxygen-ion migration in mixed ionic-electronic conducting (MIEC) perovskite oxides are thermally activated processes [36], [37], [38]. At elevated temperatures, enhanced oxygen-ion mobility within the LSCF lattice and accelerated surface exchange kinetics collectively contribute to higher overall oxygen flux. Across the entire temperature range investigated, the BYS-coated membrane consistently exhibited higher oxygen permeability than the uncoated membrane. At 950 °C, the oxygen flux improved from 1.9 mL/min·cm² (uncoated) to 2.1 mL/min·cm² (BYS-coated), representing an approximately 10.5% measurable enhancement in oxygen transport efficiency. This improvement can be attributed to the formation of a thin and uniform BYS layer with increased surface roughness (Figure 3f), which enlarges the gas-solid interface area and facilitates faster oxygen adsorption and desorption. These results are consistent with previous studies reporting that surface modification effectively enhances oxygen permeation in LSCF-based hollow fiber membranes [13], [38], [39]. The Arrhenius analysis (Figure 4b) further revealed that the activation energy (E_a) for oxygen transport dropped from 74.91 kJ/mol for the unmodified membrane to 66.45 kJ/mol for the BYS-coated sample. The reduced E_a value indicates that the BYS layer alters the rate-determining step by lowering surface exchange resistance and facilitating more rapid oxygen incorporation and release. Overall, these findings confirm that BYS surface modification effectively enhances surface kinetics and improves the oxygen permeation performance of the LSCF hollow fiber membrane.

3.2.2 Oxygen permeation using N_2O as the oxygen source

Following the verified enhancement observed for the BYS-coated membrane under air (O_2) as the oxygen feed, the coated membrane was selected for subsequent N_2O-assisted oxygen permeation experiments, consistent with the primary objective of this study to evaluate N_2O as an alternative oxygen donor. Oxygen transport under N_2O feed is likewise governed by surface reaction kinetics, particularly N_2O decomposition and subsequent oxygen incorporation into the membrane lattice. Therefore, the improvement observed under O_2 operation provides a clear mechanistic basis for focusing on the BYS-coated membrane. The oxygen transport performance of the BYS-coated 6-channel LSCF hollow fiber membrane was systematically investigated using nitrous oxide (N_2O) as the oxygen source. The effects of feed gas flow rate, sweep gas flow rate, and operating temperature on oxygen permeation behavior and catalytic N_2O decomposition efficiency were examined in detail.

3.2.2.1. Effect of feed gas (N_2O) flow rate

The influence of N_2O feed flow rate (25-100 mL/min) on oxygen permeation was examined at 980 °C, while maintaining the argon sweep gas flow rate at 100 mL/min. As shown in Figure 5, a nonlinear relationship between oxygen flux and N_2O flow rate was observed. The oxygen permeation flux increased as the N_2O flow rate increased from 25 mL/min to 50 mL/min, reaching a maximum at 50 mL/min. Nonetheless, a further increase in feed flow rate to 100 mL/min resulted in a gradual decline in oxygen flux. This behavior reflects the interplay between external mass transfer and surface reaction kinetics. At low N_2O flow rate (25 mL/min), the limited reactant supply restricts the formation of oxygen intermediates on the membrane surface, thereby constraining oxygen ion transport through the dense membrane layer. Under these conditions, external diffusion dominated, as insufficient N_2O molecules reach the active sites for efficient catalytic decomposition. Increasing the flow rate to 50 mL/min enhances the oxygen partial pressure gradient and reduces external mass transfer limitations, leading to improved oxygen flux and higher reaction efficiency [40], [41]. Beyond this optimal flow rate, however, reduced residence time becomes significant. Higher gas velocities shorten the contact time between N_2O molecules and the catalytic surface, thereby suppressing decomposition efficiency despite adequate active surface area [42]. These findings highlight the necessity of balancing reactant transport and surface kinetics to achieve optimal membrane performance. Although the BYS overlayer promotes oxygen surface exchange and ionic transport, appropriate gas flow conditions are essential to fully exploit its catalytic functionality. Under the present experimental conditions, an N_2O feed flow rate of 50 mL/min was identified as optimal, yielding the highest oxygen permeation flux at 980 °C.

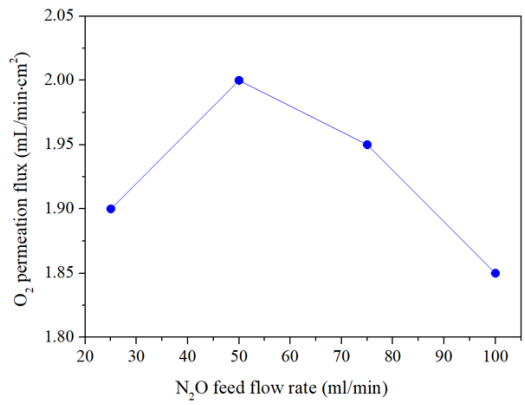

Figure 5: Oxygen permeation fluxes at various N_2O feed flow rates through the BYS-coated LSCF hollow membranes (at 980 °C and 100 mL/min of Ar sweep gas).

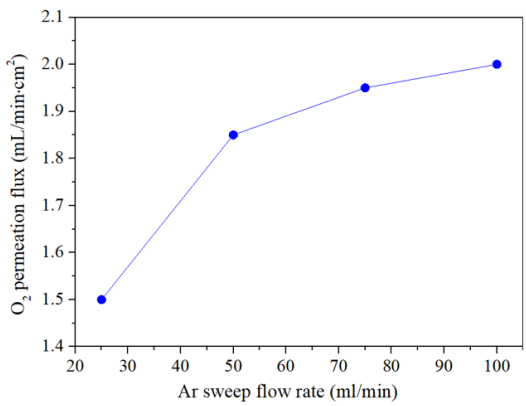

Figure 6: Oxygen permeation flux at different Ar sweep gas through the BYS-coated LSCF hollow membranes (at 980°C and 50 mL/min of N_2O feed gas).

3.2.2.2. Effect of sweep gas (Ar) flow rate

The influence of argon flow rate on oxygen transport was investigated at 980 °C while maintaining a constant N_2O feed of 50 mL/min. This evaluation aimed to clarify the role of the sweep gas in facilitating oxygen removal from the permeate side and sustaining the chemical potential gradient that drives oxygen permeation. As shown in Figure 6, the argon flow rate on the lumen side was varied from 25 to 100 mL/min. The oxygen permeation flux increased from 1.5 to 2.0 mL/min·cm^2 as the sweep gas rate was raised across this range. A measurable increase in flux was observed between 25 and 50 mL/min, rising from 1.50 to 1.85 mL/min·cm^2. At low sweep gas rates, oxygen accumulation on the permeate side elevates the local oxygen partial pressure, thereby reducing the chemical potential gradient across the membrane and diminishing the driving force for oxygen ion transport. Increasing the Ar flow rate effectively dilutes and removes the permeated oxygen, maintaining a low oxygen partial pressure on the permeate side and enhancing the oxygen transport rate [39].

In contrast, further increases in sweep gas flow to 75 and 100 mL/min resulted in only marginal improvements, with flux values of 1.95 and 2.00

mL/min·cm^2, respectively. This plateau behavior suggests that, at higher sweep rates, oxygen transport becomes limited by the intrinsic bulk diffusion and surface exchange kinetics of the BYS-coated LSCF membrane rather than by external mass transfer. From a practical perspective, these findings underscore the importance of optimizing sweep gas flow rate to balance separation performance and operational efficiency. Insufficient sweep gas flow suppresses oxygen permeation due to reduced driving force, whereas excessive flow increases gas consumption with minimal additional gain in flux. Therefore, identifying an optimal sweep gas rate is essential for achieving high oxygen separation efficiency while maintaining energy and economic feasibility in membrane reactor applications.

3.2.2.3. Effect of temperature

The effect of temperature on oxygen permeation and catalytic N_2O decomposition was studied using 50 mL/min of N_2O on the shell side and 100 mL/min of Ar on the lumen side. As illustrated in Figure 7(a), the oxygen permeation flux increased significantly from 0.6 mL/min·cm^2 at 900 °C to 2.0 mL/min·cm^2 at 980 °C. Simultaneously, N_2O conversion rose from 38% to 80%, indicating a strong correlation between oxygen permeation rate and catalytic decomposition activity. The pronounced temperature dependence can be attributed to two coupled effects. First, elevated temperatures accelerate the kinetics of N_2O decomposition, increasing the oxygen partial pressure on the feed side and generating a higher concentration of adsorbed oxygen species (O*). Second, higher temperatures enhance oxygen ion diffusion within the LSCF lattice and promote faster oxygen recombination and desorption at the BYS-coated surface. Because N_2O decomposition ($N_2O \rightleftharpoons N_2 + O^*$) is an endothermic reaction, increasing temperature thermodynamically favors oxygen formation. Meanwhile, continuous oxygen removal by the Ar sweep gas maintains a low oxygen partial pressure on the permeate side, thereby reinforcing the chemical potential gradient that drives oxygen ion transport. The nearly linear increase in oxygen flux with temperature indicates that the process remained thermally activated throughout the studied range, without reaching diffusion-limited saturation. The concurrent increase in oxygen flux and N_2O conversion further indicates a coupled, self-enhancing mechanism: continuous oxygen removal shifts the decomposition equilibrium forward, consistent with Le Châtelier's principle, thereby sustaining high oxygen activity at the feed-membrane interface. This feedback effect explains the strong correlation observed between oxygen permeation and N_2O conversion.

A comparison between air and N_2O as oxygen sources reveals distinct enhancement mechanisms. When air is used, the BYS layer primarily reduces the activation barrier for surface oxygen exchange, leading to improved flux across the temperature range. In contrast, under N_2O feed, the membrane not only enhances surface oxygen kinetics but also integrates in situ catalytic decomposition with continuous oxygen removal, resulting in simultaneous increases in

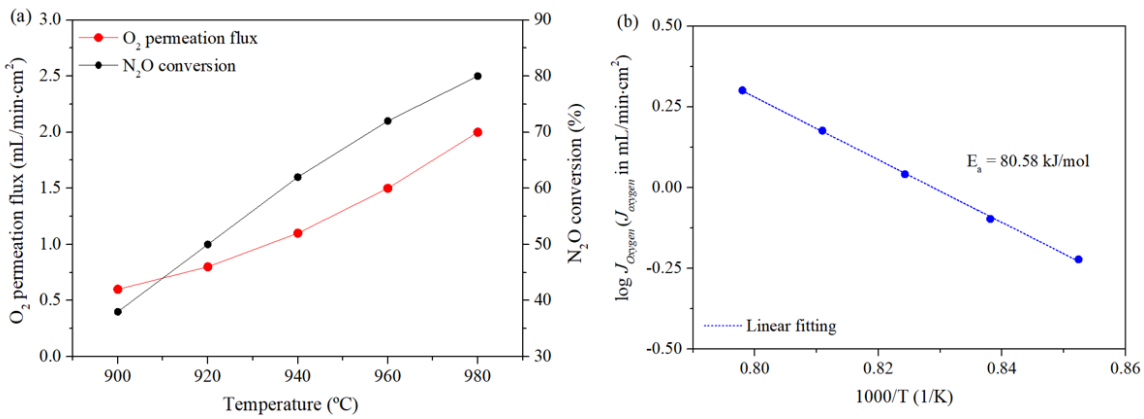

Figure 7: **(a)** Oxygen permeation flux and N_2O conversion using the BYS-coated LSCF hollow membranes at various temperatures (900-980 °C). **(b)** Arrhenius plots of the oxygen permeation flux for BYS-coated LSCF hollow membranes at different temperatures (900-980 °C) (100 mL/min of Ar sweep gas and 50 mL/min of N_2O feed gas).

oxygen flux and N_2O conversion. At temperatures above 950 °C, both systems showed optimal performance, with maximum oxygen flux and efficient N_2O decomposition without evident mass transfer limitations. Nevertheless, oxygen flux under air remained consistently higher than that under N_2O, since N_2O must first undergo catalytic decomposition before oxygen ions can be transported through the membrane. Arrhenius analysis showed that apparent activation energy under N_2O feed (80.58 kJ/mol, Figure 7b) was higher than that obtained with air (66.45 kJ/mol, Figure 4b), reflecting the additional energetic requirement imposed by the N_2O decomposition step.

These results demonstrate that the BYS-coated LSCF hollow fiber membrane can effectively operate with both conventional (O_2) and alternative (N_2O) oxygen sources. Although air enables higher oxygen fluxes, the use of N_2O provides a dual functional advantage by coupling oxygen production with greenhouse gas mitigation. A comparative summary of oxygen permeation fluxes for coated and uncoated membranes, together with literature data, is presented in Table 1.

3.3 Mechanism of oxygen permeation through membrane

The oxygen permeation behavior of the membrane can be fundamentally interpreted based on the oxygen chemical potential gradient established across the membrane thickness, as widely described for mixed ionic-electronic conducting (MIEC) membranes in previous studies [44]. The driving force for oxygen transport is governed by the difference in oxygen partial pressure (pO_2) between the feed and permeate sides. Under the present conditions, continuous removal of oxygen by the Ar sweep gas effectively lowers the pO_2 at the permeate side, thereby sustaining a strong chemical potential gradient that promotes oxygen ion migration through the LSCF lattice. Any increase in the permeate-side oxygen concentration would reduce this gradient and consequently suppress the permeation flux. The overall oxygen transport process involves multiple sequential steps, including (i) adsorption and dissociation of molecular oxygen (or oxygen species generated from N_2O decomposition) at the membrane surface, (ii) incorporation of oxygen into the lattice as O^{2-} ions, (iii) bulk diffusion of oxygen ions and electron holes through the mixed ionic-electronic conducting LSCF structure, and (iv) recombination and desorption of oxygen molecules at the permeate side. Depending on temperature and operating conditions, the rate-limiting step may shift between surface exchange kinetics and bulk diffusion. The observed increase in flux with temperature suggests thermally activated transport, consistent with enhanced oxygen ion mobility and accelerated surface reaction kinetics.

The introduction of the BYS coating further modifies the surface reaction environment. Owing to its high oxygen ion conductivity and catalytic activity, the BYS layer facilitates faster surface oxygen exchange by lowering the activation barrier for oxygen dissociation and incorporation into the LSCF lattice. In the case of N_2O feed, the BYS coating also promotes in situ

Table 1: Comparison of the oxygen permeation fluxes of hollow fiber membranes obtained from this work with other literature.

Membrane Type	Temperature (°C)	O_2 Flux (mL/min·cm^2)	Feed/Sweep gas	Ref.
LSCF hollow fiber	950	1.90	Air/Ar	This work
LSCF hollow fiber with BYS coating	950	2.10	Air/Ar	This work
LSCF hollow fiber with BYS coating	980	2.00	N_2O/Ar	This work
LSCF hollow fiber	900	~1.05	Air/Ar	[43]
Multi-bore LSCF capillary membrane	950	1.39	Air/Ar	[33]
LSCF with BSCN coating	950	1.92	Air/He	[38]
Single LSCF hollow fiber	950	0.26	Air/Ar	[40]

catalytic decomposition of N_2O ($N_2O \rightleftharpoons N_2 + O^*$), increasing the local availability of reactive oxygen species at the membrane surface. This synergistic interaction between catalytic decomposition and membrane transport enhances the effective oxygen activity at the interface and supports sustained oxygen permeation. However, the higher apparent activation energy observed for N_2O compared with air has been interpreted in terms of the additional energy barrier associated with N_2O dissociation prior to oxygen incorporation into the LSCF lattice.

4 Conclusions

In this work, a 6-channel LSCF hollow fiber membrane was successfully fabricated via a phase inversion-sintering method and subsequently modified through in situ deposition of a BYS overlayer. The BYS coating was uniformly distributed along the internal channel surfaces, increasing surface roughness and enlarging the active interfacial area available for oxygen exchange. Structural and morphological characterizations (XRD and SEM) confirmed that the coating process preserved the crystalline integrity of the LSCF framework while imparting enhanced surface functionality. The modified membrane demonstrated effective oxygen permeation using both conventional (air) and alternative (N_2O) oxygen sources. Higher oxygen fluxes were consistently obtained when air was used as the feed gas, owing to the direct diffusion of molecular oxygen across the membrane. In contrast, lower fluxes under N_2O feed were attributed to the additional catalytic decomposition step required to generate oxygen prior to ionic transport. Under optimized operating conditions (980 °C, 50 mL/min N_2O on the shell side and 100 mL/min Ar as the sweep gas), the membrane achieved a maximum oxygen flux of approximately 2.0 mL/min·cm^2. The enhanced transport performance was primarily attributed to the synergistic interaction between the LSCF lattice and the BYS coating, which reduced surface exchange resistance and promoted oxygen ion mobility. Overall, the BYS-coated LSCF hollow fiber membrane exhibits strong potential for application in membrane reactor systems for energy and environmental processes. Its capability to provide a controllable and spatially distributed oxygen supply makes it particularly attractive for reactions such as oxidative coupling of methane (OCM), partial oxidation of hydrocarbons, and syngas production. It should be acknowledged that long-term stability factors, including coating adhesion, potential bismuth volatility at elevated temperatures, and resistance to thermal cycling, were not systematically investigated in the present study. These aspects may affect the practical implementation of Bi_2O_3-based surface modifications and therefore warrant further investigation in future work. Importantly, integrating N_2O decomposition with membrane-assisted oxygen separation offers a dual benefit: efficient oxygen delivery coupled with greenhouse gas mitigation, contributing to more sustainable energy conversion strategies.

Acknowledgments

This research has received funding support from King Mongkut's University of Technology North Bangkok; KMUTNB (contract number KMUTNB-FF-67-B-23), National Research Council of Thailand; NRCT (contract number N83A670023, N84A680761 and N84A680934), Program Management Unit for Competitiveness; PMUC (contact number C23F670095) and the International Science Partnerships Fund (ISPF via the British Council).

Author Contributions

I.S., K.L. and U.W.H: Conceptualization; V.T. and C.K.: methodology; V.T., N.S., R.T. and A.M.: validation; V.T., C.K., P.M., R.T. and A.M.: formal analysis; V.T, C.K. and P.M.: investigation; I.S. and U.W.H.: resources; V.T., R.T and A.M.: data curation; V.T. and R.T.: writing—original draft preparation; I.S., K.L., M.H., U.W.H. and A.M.: writing—review and editing; A.M.: visualization; U.W.H. and A.M.: supervision; I.S., N.S. and U.W.H.: project administration; I.S. and U.W.H.: funding acquisition. All authors have read and agreed to the published version of the manuscript.

Conflicts of Interest

The authors declare no conflicts of interest.

Declaration of generative AI and AI-assisted technologies in the writing process

The authors have not utilised any generative AI tool for any assistance in the writing process.

References

[1] M. Thanasiriruk, P. Saychoo, C. Khajonvittayakul,

V. Tongnan, U. W. Hartley, and N. Laosiripojana, "Optimizing operating conditions for Oxidative Coupling Methane (OCM) in the presence of NaCl-MnO_x/SiO_2," *Applied Science and Engineering Progress*, vol. 14, no. 3, pp. 477–488, 2021, doi: 10.14416/j. asep.2020.10.001.

[2] Y. Lu, A. G. Dixon, W. R. Moser, Y. H. Ma, and U. Balachandran, "Oxygen-permeable dense membrane reactor for the oxidative coupling of methane," *Journal of Membrane Science*, vol. 170, no. 1, pp. 27–34, 2000, doi: 10.1016/S0376-7388(99)00354-3.

[3] J. E. ten Elshof, H. J. M. Bouwmeester, and H. Verweij, "Oxidative coupling of methane in a mixed-conducting perovskite membrane reactor," *Applied Catalysis A: General*, vol. 130, no. 2, pp. 195–212, 1995, doi: 10.1016/0926-860X(95)00098-4.

[4] H. Wang, Y. Cong, and W. Yang, "Continuous oxygen ion transfer medium as a catalyst for high selective oxidative dehydrogenation of ethane," *Catalysis Letters*, vol. 84, no. 1–2, pp. 101–106, 2002, doi: 10.1023/A:1021088904379.

[5] U. Balachandran et al., "Ceramic membrane reactor for converting methane to syngas," *Catalysis Today*, vol. 36, no. 3, pp. 265–272, 1997, doi: 10.1016/S0920-5861(96)00229-5.

[6] X. Tan and K. Li, "Applications of dense ceramic membrane reactors in selected oxidation and dehydrogenation processes for chemical production," in *Handbook of Membrane Reactors*, UK: Woodhead, 2013, pp. 347–383, vol. 2, doi: 10.1533/9780857097347.2.347.

[7] G. Chen et al. "Perspectives on achievements and challenges of oxygen transport dual-functional membrane reactors," *Journal of the American Ceramic Society*, vol. 107, no. 3, pp. 1490–1504, 2024, doi: 10.1111/jace.19411.

[8] J. Sunarso, S. S. Hashim, N. Zhu, and W. Zhou, "Perovskite oxides applications in high temperature oxygen separation, solid oxide fuel cell and membrane reactor: A review," *Progress in Energy and Combustion Science*, vol. 61, pp. 57–77, 2017, doi: 10.1016/j.pecs.2017.03.003.

[9] H. Liu et al., "Enhanced oxygen permeation through perovskite hollow fibre membranes by methane activation," *Ceramics International*, vol. 35, no. 4, pp. 1435–1439, 2009, doi: 10.1016/j.ceramint.2008.07.011.

[10] Y. Teraoka, H.-M. Zhang, and N. Yamazoe, "Oxygen-Sorptive Properties Of Defect Perovskite-Type $La_{1-x}Sr_xCo_{1-y}Fe_yO_{3-\delta}$," *Chemistry Letters*, vol. 14, no. 9, pp. 1367–1370, 1985, doi: 10.1246/cl.1985.1367.

[11] X. Tan, Y. Liu, and K. Li, "Preparation of LSCF ceramic hollow-fiber membranes for oxygen production by a phase-inversion/sintering technique," *Industrial and Engineering Chemistry Research*, vol. 44, no. 1, pp. 61–66, 2005, doi: 10.1021/ie040179c.

[12] H. Pan, L. Li, X. Deng, B. Meng, X. Tan, and K. Li, "Improvement of oxygen permeation in perovskite hollow fibre membranes by the enhanced surface exchange kinetics," *Journal of Membrane Science*, vol. 428, pp. 198–204, 2013, doi: 10.1016/j.memsci.2012.10.020.

[13] X. Tan, Z. Wang, H. Liu, and S. Liu, "Enhancement of oxygen permeation through $La_{0.6}Sr_{0.4}Co_{0.2}Fe_{0.8}O_{3-\delta}$ hollow fibre membranes by surface modifications," *Journal of Membrane Science*, vol. 324, no. 1–2, pp. 128–135, 2008, doi: 10.1016/j.memsci.2008.07.008.

[14] A. Leo, S. Liu, J. C. Diniz da Costa, and Z. Shao, "Oxygen permeation through perovskite membranes and the improvement of oxygen flux by surface modification," *Science and Technology of Advanced Materials*, vol. 7, no. 8, pp. 819–825, 2006, doi: 10.1016/j.stam.2006.11.013.

[15] Y. Teraoka, Y. Honbe, J. Ishii, H. Furukawa, and I. Moriguchi, "Catalytic effects in oxygen permeation through mixed-conductive LSCF perovskite membranes," *Solid State Ionics*, vol. 152–153, pp. 681–687, 2002, doi: 10.1016/S0167-2738(02)00409-5.

[16] M. Alizadeh, A. Maghsoudipour, and K. Ahmadi, "Phase stability and conductivity of δ-Bi_2O_3 with mixture of yttrium and ytterbium oxides," *International Journal of Engineering, Transactions A: Basics*, vol. 25, no. 2, pp. 159–164, 2012, doi: 10.5829/idosi.ije.2012.25.02a.05.

[17] C. L. Gomez et al., "Stabilization of the delta-phase in Bi_2O_3 thin films," *Solid State Ionics*, vol. 255, pp. 147–152, 2014, doi: 10.1016/j.ssi.2013.12.027.

[18] G. A. Mutch, L. Qu, G. Triantafyllou, W. Xing, M. L. Fontaine, and I. S. Metcalfe, "Supported molten-salt membranes for carbon dioxide permeation," *Journal of Materials Chemistry A*, vol. 7, no. 21, pp. 12951–12973, 2019, doi: 10.1039/c9ta01979k.

[19] N. H. Othman, Z. Wu, and K. Li, "A micro-structured $La_{0.6}Sr_{0.4}Co_{0.2}Fe_{0.8}O_{3-\delta}$ hollow fibre membrane reactor for oxidative coupling of methane," *Journal of Membrane Science*, vol.

468, pp. 31–41, 2014, doi: 10.1016/j.memsci.2014.05.051.

[20] N. H. Othman, Z. Wu, and K. Li, "An oxygen permeable membrane microreactor with an in-situ deposited $Bi_{1.5}Y_{0.3}Sm_{0.2}O_{3-\delta}$ catalyst for oxidative coupling of methane," *Journal of Membrane Science*, vol. 488, pp. 182–193, 2015, doi: 10.1016/j.memsci.2015.04.027.

[21] Y. Li, X. Wang, and C. Shi, "The catalytic performance of Ba-Ce-Cu catalysts for N_2O decomposition," *Journal of Environmental Chemical Engineering*, vol. 11, no. 3, 2023, doi: 10.1016/j.jece.2023.109970.

[22] M. F. Alhasan, K. M. Alanezi, S. A. S. Alali, M. A. Al-Ebrahim, S. Bunian, and A. A. Nour, "Thermal-hydraulic characteristics of nitric acid: An experimental and numerical analysis," *Heliyon*, vol. 10, no. 1, Art no. e23089, 2024, doi: 10.1016/j.heliyon.2023.e23089.

[23] L. E. Revell, F. Tummon, R. J. Salawitch, A. Stenke, and T. Peter, "The changing ozone depletion potential of N_2O in a future climate," *Geophysical Research Letters*, vol. 42, no. 22, pp. 10047–10055, 2015, doi: 10.1002/2015GL065702.

[24] Y. Li et al., "Increased nitrous oxide emissions from global lakes and reservoirs since the pre-industrial era," *Nature Communications*, vol. 15, no. 1, pp. 1–11, 2024, doi: 10.1038/s41467-024-45061-0.

[25] Z. Zhuang et al., "Review of nitrous oxide direct catalytic decomposition and selective catalytic reduction catalysts," *Nature Communications*, vol. 486, no. 800, Art no. 150374, 2024, doi: 10.1016/j.cej.2024.150374.

[26] M. Liu, Z. Cao, W. Liang, Y. Zhang, and H. Jiang, "Membrane catalysis: N_2O decomposition over $La_{0.2}Sr_{0.8}Ti_{0.2}Fe_{0.8}O_{3-\delta}$ membrane with oxygen permeability," *Chemie-Ingenieur-Technik*, vol. 94, no. 1–2, pp. 70–77, 2022, doi: 10.1002/cite.202100122.

[27] R. Akoumeh, M. Al-Ejji, B. Aljaoni, and M. Abbas, "Advances in ceramic membrane technology: Versatility of fabrication technique, industrial applications, and challenges," *Inorganic Chemistry Communications*, vol. 179, no. P1, Art no. 114685, 2025, doi: 10.1016/j.inoche.2025.114685.

[28] X. Tao et al., "Facile microwave-assisted synthesis of Ce-doped Bi_2O_3 for efficient hybrid supercapacitors," *Battery Energy*, vol. 3, no. 2, pp. 1–12, 2024, doi: 10.1002/bte2.20230052.

[29] Z. Wu, D. Zeng, X. Liu, C. Yu, K. Yang, and M. Liu, "Hierarchical δ-Bi_2O_3/$Bi_2O_2CO_3$ composite microspheres: phase transformation fabrication, characterization and high photocatalytic performance," *Research on Chemical Intermediates*, vol. 44, no. 10, pp. 5995–6010, 2018, doi: 10.1007/s11164-018-3471-4.

[30] M. Zawadzki and J. Trawczyński, "Synthesis, characterization and catalytic performance of LSCF perovskite for VOC combustion," *Catalysis Today*, vol. 176, no. 1, pp. 449–452, 2011, doi: 10.1016/j.cattod.2010.10.070.

[31] C. Yacou, J. Sunarso, C. X. C. Lin, S. Smart, S. Liu, and J. C. Diniz da Costa, "Palladium surface modified $La_{0.6}Sr_{0.4}Co_{0.2}Fe_{0.8}O_{3-\delta}$ hollow fibres for oxygen separation," *Journal of Membrane Science*, vol. 380, no. 1–2, pp. 223–231, 2011, doi: 10.1016/j.memsci.2011.07.008.

[32] X. Nie et al., "The sintering temperature effect on electrochemical properties of $Ce_{0.8}Sm_{0.05}Ca_{0.15}O_{2-\delta}$ (SCDC)-$La_{0.6}Sr_{0.4}Co_{0.2}Fe_{0.8}O_{3-\delta}$ (LSCF) heterostructure pellet," *Nanoscale Research Letters*, vol. 14, 2019, doi: 10.1186/s11671-019-2979-x.

[33] Y. Chi, T. Li, B. Wang, Z. Wu, and K. Li, "Morphology, performance and stability of multi-bore capillary $La_{0.6}Sr_{0.4}Co_{0.2}Fe_{0.8}O_{3-\delta}$ oxygen transport membranes," *Journal of Membrane Science*, vol. 529, pp. 224–233, Jan. 2017, doi: 10.1016/j.memsci.2017.02.010.

[34] Y. Liu et al., "Performance study of asymmetric oxygen transport membranes with vertically channelled pores by phase inversion tape casting," *Open Ceramics*, vol. 9, p. 100248, Feb. 2022, doi: 10.1016/j.oceram.2022.100248.

[35] B. T. Na, J. H. Park, J. H. Park, J. H. Yu, and J. H. Joo, "Elucidation of the Oxygen Surface Kinetics in a Coated Dual-Phase Membrane for Enhancing Oxygen Permeation Flux," *ACS Applied Materials and Interfaces*, vol. 9, no. 23, pp. 19917–19924, 2017, doi: 10.1021/acsami.7b04685.

[36] J. Yang, H. Zhao, X. Liu, Y. Shen, and L. Xu, "Bismuth doping effects on the structure, electrical conductivity and oxygen permeability of $Ba_{0.6}Sr_{0.4}Co_{0.7}Fe_{0.3}O_{3-\delta}$ ceramic membranes," *International Journal of Hydrogen Energy*, vol. 37, no. 17, pp. 12694–12699, 2012, doi: 10.1016/j.ijhydene.2012.06.013.

[37] A. Subardi, C. C. Chen, and Y. P. Fu, "Oxygen transportation, electrical conductivity and electrochemical properties of layered perovskite $SmBa_{0.5}Sr_{0.5}Co_2O_{5+\delta}$," *International Journal of Hydrogen Energy*, vol. 42, no. 8, pp. 5284–5294, 2017, doi: 10.1016/j.ijhydene.2016.11.123.

[38] D. Han, J. Wu, Z. Yan, K. Zhang, J. Liu, and S.

Liu, "$La_{0.6}Sr_{0.4}Co_{0.2}Fe_{0.8}O_{3-\delta}$ hollow fibre membrane performance improvement by coating of $Ba_{0.5}Sr_{0.5}Co_{0.9}Nb_{0.1}O_{3-\delta}$ porous layer," *RSC Advances*, vol. 4, no. 38, pp. 19999–20004, 2014, doi: 10.1039/c4ra00704b.

[39] M. Lee, Y. Gan, C. Yang, C. Ren, and X. Xue, "Fabrication and accelerated long-term stability test of asymmetrical hollow fiber-supported thin film oxygen separation membrane," *Journal of Membrane Science*, vol. 655, Art no. 120600, Apr. 2022, doi: 10.1016/j.memsci.2022.120600.

[40] Y. Hu et al., "Perovskite hollow fiber membranes supported in a porous and catalytically active perovskite matrix for air separation," *Separation and Purification Technology*, vol. 192, pp. 435–440, Oct. 2018, doi: 10.1016/j.seppur.2017.10.037.

[41] J. Sunarso et al., "Mixed ionic-electronic conducting (MIEC) ceramic-based membranes for oxygen separation," *Journal of Membrane Science*, vol. 320, no. 1–2, pp. 13–41, 2008, doi: 10.1016/j.memsci.2008.03.074.

[42] B. Moszowski, M. Mulica-Musiał, P. J. Piszko, and M. Dobrzyński, "The Behavior of Catalytic, Low-Temperature N_2O Decomposition (LT-deN_2O) in the Presence of Sulfur-Containing Compounds on Nitric Acid Plants," *Applied Sciences*, vol. 14, no. 20, 2024, doi: 10.3390/app14209353.

[43] K. Li, X. Tan, and Y. Liu, "Single-step fabrication of ceramic hollow fibers for oxygen permeation," *Journal of Membrane Science*, vol. 272, no. 1–2, pp. 1–5, 2006, doi: 10.1016/j.memsci.2005.11.053.

[44] A. H. Alami, A. Alashkar, M. A. Abdelkareem, H. Rezk, M. S. Masdar, and A. G. Olabi, "Perovskite Membranes: Advancements and Challenges in Gas Separation, Production, and Capture," *Membranes*, vol. 13, no. 7, pp. 661-689, 2023, doi: 10.3390/membranes13070661.